Discontinuities Formed in Inconel GTA Welds

Aluminum segregation, niobium enrichment and a gap between nil-strength and solidus temperatures each played a role in the weld cracking problems

BY R. A. PATTERSON, R. B. NEMEC AND R. D. REISWIG

ABSTRACT. Autogenous gas tungsten arc welds between Inconel[1] 625 (NO6625) and Inconel[1] 600 (NO6600) were found to be susceptible to three principal discontinuity forms: (1) oxide tails extending from the weld root, (2) liquation zone cracking in the weld underbead region, and (3) liquation zone porosity in the weld underbead region. Examination of these discontinuity types has been performed and their occurrence correlated with material composition irregularities and welding procedure characteristics.

Oxide tails were shown to be coincident with aluminum segregation to interfaces like the unfused region of a lap joint. Corrective measures for the elimination of oxide tails were evaluated with respect to a specific welding application.

Liquation zone cracking was the most deleterious discontinuity encountered during this work. Analysis of the crack regions indicated that the decomposition of precipitates in Alloy NO6625 (primarily Nb-, Ti- and Mo-based carbides) was linked with cracking. Niobium was identified as the most significant segregating element associated with the cracking event.

Liquation-zone shrinkage porosity formed due to circumstances similar to those accompanying the liquation-zone cracking discontinuities. Niobium segregation was the predominant compositional effect.

Differential thermal analysis of the NO6625, NO6600 and weld metal indicated that the NO6625 composition had the largest liquidus/solidus phase separation, combined with the lowest solidus temperature, and as such, would be the most susceptible to the formation of a partially melted zone (liquation). Hot strength testing of the NO6625 alloy indicated that the nil-strength temperature was approximately 40°C (72°F) below the solidus temperature. These data thus indicated that the NO6625 alloy would be susceptible to hot cracking. This susceptibility, in conjunction with the analysis of the discontinuities, supports a hot cracking mechanism for the formation of the liquation-zone cracks.

Paper presented at the 66th Annual AWS Meeting, held April 28 through May 3, 1985, in Las Vegas, Nev.

R. A. PATTERSON, R. B. NEMEC and R. D. REISWIG are with the Materials Science and Technology Division, Los Alamos National Laboratory, Los Alamos, N. Mex.

[1]Commercial trademark of the INCO family of companies.

Introduction

During the welding of nuclear fuel elements for the Transient Reactor Test Facility[2] (TREAT) Upgrade program, difficulties were encountered relating to the effects and occurrence of several types of discontinuities[3]: oxide tails, liquation-zone cracks and liquation-zone porosity. Since the intended use of the nuclear fuel elements imposed extreme conditions on the welds (high temperature cycles with large thermal gradients and air exposure), stringent quality assurance requirements were placed upon the assemblies. Figure 1 is a nuclear fuel element schematic showing the central region of graphite-uranium dioxide fuel, surrounded by graphite reflectors and encapsulated in a hermetic metal cladding. Alloy NO6625 was selected for the clad material based upon high-temperature strength and oxidation resistance. Alloy NO6600 was selected for the end fittings due to reduced temperature exposure. Autogenous gas tungsten arc welding was selected as the technique to join the NO6625 clad structure to the NO6600 end fittings.

Figure 2 shows that the geometry of the clad structure was that of a thin (6.35-mm/0.25-in.) square pipe (10 cm (4 in.) flat by 2.7 m (8.8 ft) long). The end fitting had a land, which was pressed into the cladding, and the raised reinforcement located the cladding and served as a consumable during welding—Fig. 2. Welding was done with the fuel element in the vertical position, using the pulsed current gas tungsten arc (GTAW-P) process with robotic torch manipulation. Welding variables (Table 1) were sequenced by computer control, using either time reference from the weld power supply computer or position reference from the robot computer. All welding was thus done to a predeveloped procedure and kept constant within the control limits of the welding power supply and computer controls. Therefore, the incidence of discontinuities should have been a function of uncontrollable variables (*e.g.*, variations in material composition and set-up procedures). Figure 3 shows a typical cladding-to-end-fitting weld with the weld fixturing and the torch positioned (45-deg

[2]Research reactor operated by Argonne National Laboratory.

[3]It is to be noted that, under specific conditions of fitness for service, the discontinuities described in this paper may also be considered as defects.

KEY WORDS
Nickel Alloy Welds
Inconel 625-600 Weld
NO6625-NO6600 Welds
Oxide Tails
Liquation Zone Crack
Liquation Solidifying
Underbead Porosity
Nuclear Weld Defects
Thermal Analysis
Pulsed Current GTAW

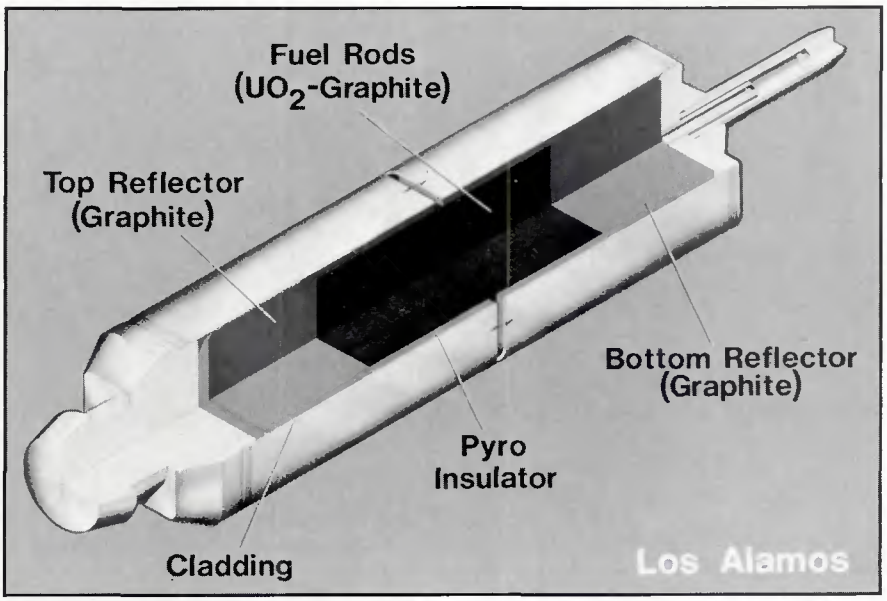

Fig. 1—Schematic of the TREAT fuel element

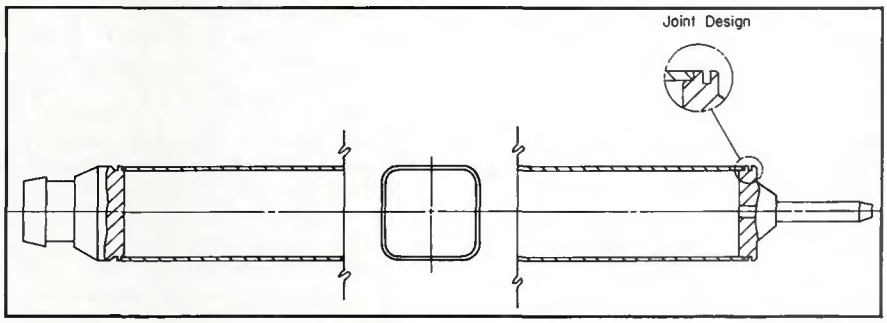

Fig. 2—Schematic of the TREAT fuel element cladding showing the end-fitting-to-cladding weld joint design

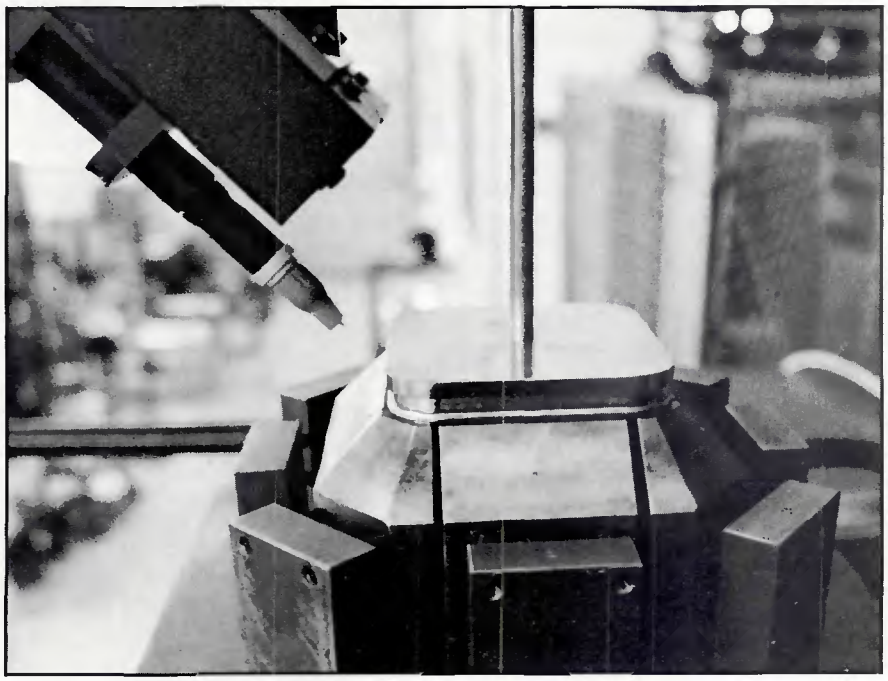

Fig. 3—Photograph of a representative end-fitting-to-cladding weld with the weld fixture and welding torch positioned according to procedure

Table 1—Weld Schedule

Weld current	
High pulse value	85A
Low pulse value	20A
Pulse frequency (2.5 Hz)	
High pulse duration	0.2 s
Low pulse duration	0.2 s
Arc voltage control potential	13.4 V
Weld travel speed	2.5 mm/s
Shielding gas (pure Ar)	40 cfh
Electrode	W-2 wt-% Th 1.6-mm diameter 30-deg included angle with 0.5-mm blunt
Power supply	direct current electrode negative

approach angle) as called for in the weld procedure.

Nickel-based alloys have reportedly been very susceptible to welding discontinuities and are oftentimes subjected to very stringent measures in attempts to avoid these discontinuities. Prager and Shira (Ref. 1) published a thorough review of this subject, indicating that these alloys are susceptible to microfissuring, hot cracking, porosity, and strain age cracking, to mention a few. In the present study, three principal discontinuity types were analyzed: oxide tails, liquation-zone cracking, and liquation-zone shrinkage porosity. The majority of the literature reviewed dealt with discontinuities formed in the precipitation-hardened nickel-based alloys. This report will draw upon this previously reported data to illustrate the mechanisms for discontinuity formation in NO6625 welds.

Materials

Table 2 lists the compositions for NO6600, NO6625 and the weld metal, which shows an approximate 25% dilution of NO6625 in the weld composition. Review of the compositions reveals that these alloys were within normal commercial specification limits, with the exception of the NO6625, where the Al concentration was high. The heat of NO6625 used in this program was produced by air melting and has not been given the normal vacuum reprocessing typical of the higher quality materials.

Metallographic examination of the NO6625 alloy showed that a heavy precipitate content in the form of stringers was apparent—Fig. 4. Examination of these precipitates by energy-dispersive x-ray spectroscopy (EDS) in the scanning electron microscope (SEM) indicated that they were primarily composed of Nb, Mo

Table 2—Material Compositions[a]

	NO6625 wt-%	NO6600 wt-%	Weld Metal wt-%
Ni	62 (bal.)	75 (72)	72
Cr	21 (20–23)	16 (14–17)	17
Fe	3.8 (5)	9.6 (6–10)	8.1
Nb	3.5 (3–4)	<0.05	0.89
Mo	9.9 (8–10)	0.13	2.6
Al	1.7 (0.4)	2.1	0.94
Ti	0.23 (0.4)	0.36	0.29
C	0.05 (0.1)	0.07 (0.15)	0.06
Si	0.10 (0.5)	0.01 (0.5)	0.06
S	<0.005 (0.015)	<0.005 (0.015)	<0.005
P	<0.005 (0.015)	<0.003	<0.005
B	0.004	0.009	0.007

[a]Parentheses indicate specification maximum or range per Ref. 3.

Table 3—Differential Thermal Analysis[a]

	Solidus (°C)	Liquidus (°C)
NO6600	1328 (1355)	1355 (1410)
NO6625	1288 (1287)	1325 (1348)
Weld metal	1318	1345

[a]Ref. 3 values in parentheses.

and Ti, presumably in the form of carbides. Morphology revealed by optical metallography substantiated this premise. Analysis also revealed that the aluminum concentration associated with these precipitate stringers was higher than the bulk analysis, and ranges upwards by several percent (qualitative peak height determination).

Grain size was determined according to ASTM E112 (Ref. 2). The NO6625 grain size was ASTM 5.5 (55 μm). No significant grain coarsening was observed adjacent to the weld. The NO6600 grain size was ASTM 7 to 8 (22 to 32 μm), and increased to ASTM 3 to 5 (65 to 125 μm) adjacent to the weld.

Differential thermal analysis (DTA) of the NO6600, NO6625 and weld metal revealed that the NO6625 base metal had the broadest solidus/liquidus phase separation and lowest solidus temperature (1288° to 1335°C/2350° to 2435°F). Table 3 itemizes the DTA results for these alloys and, where applicable, reports data from the metal supplier (Ref. 3). Comparison of the DTA results reveals a fair correlation in the melting characteristics of the alloy heats used in this program with those reported for commercial alloys.

High-temperature strength tests performed on a Gleeble 1500 testing machine indicated that the NO6625 alloy had a nil-strength temperature of 1250°C (2282°F). Since the solidus of this alloy was approximately 1290°C (2354°F), there was an approximate 40°C (72°F) gap between the solidification temperature and the temperature at which the alloy could withstand significant stress.

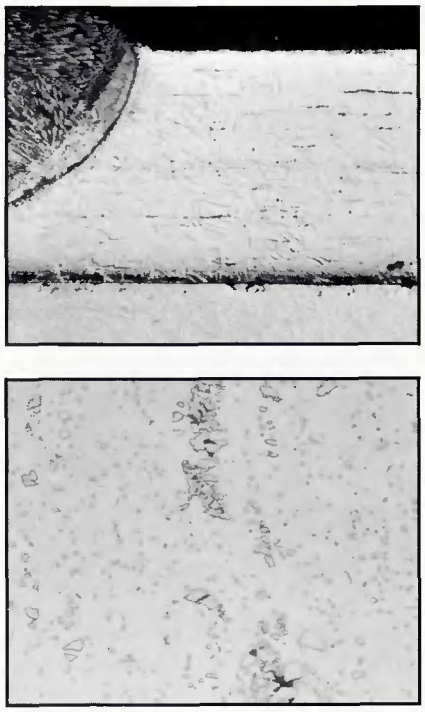

Fig. 4 — A — Photomicrograph of the Alloy NO6625 showing the annealed microstructure with extensive stringers (100 X). B — High magnification photomicrograph showing the precipitate morphologies: heaviest concentration of blocky Nb- and Mo-rich precipitates with a small concentration of angular Ti-rich precipitates (1000 X)

Discontinuity Examination

Oxide tails were the most prevalent discontinuity type within this welding program. Figure 5 shows a typical oxide tail extending from the weld root into the weld fusion zone. Notice that the morphology of this discontinuity is very reminiscent of a crack, and in fact these discontinuities are often mistaken for root cracks.

Figure 6A is a SEM photomicrograph of another representative oxide tail (cross-sectional view) showing a combination of crack-like and spherical-porosity-like morphologies. Analysis by SEM-EDS of this discontinuity region revealed that the oxide tail was primarily made up of an aluminum-rich stringer, which even extended into what appears to be the original lap interface between the cladding and end fitting — Fig. 6B.

Longitudinal views of the oxide tails revealed that they run along the weld root a distance that is several multiples of their cross-sectional length — Fig. 7. Electron microprobe (EM) analysis of these areas revealed that, compared to the primary dendrite composition (Position 2 — Fig. 7B), the interdendritic composition (Position 3 — Fig. 7B) was enriched with Nb and Mo, while the oxide tail core (Position 1 — Fig. 7B) was enriched with Al, O, Ti and Mg.

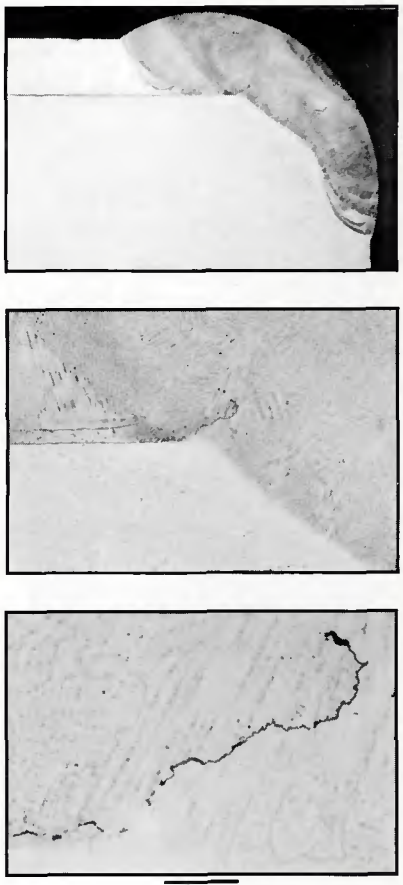

Fig. 5 — Cross-sectional photomicrographs of a representative end-fitting-to-cladding weld showing a typical oxide tail extending from the weld root. Top — 25X; Middle — 100X; Bottom — 500X.

Liquation-zone cracking was the discontinuity which produced the major difficulty during this program, even though the occurrence was much less frequent than the formation of oxide tails. The cracks were, in all instances, located in the NO6625 partially melted zone and thought to originate at the clad inner wall (weld underbead region). Figure 8 illustrates this type of discontinuity in relationship to a macroscopic view of the typical weld cross-section. Since these discontinuities could not be located by standard nondestructive test methods, their presence was only detected when the crack propagated to the clad surface and produced a helium leak indication. Once an indication of a leak was found, location of the actual crack was still extremely difficult, due to the fact that only a very small pinhole typified the crack exit point on the clad outer wall. Fluorescent dye penetrant inspection and SEM examination were then used to pinpoint suspicious

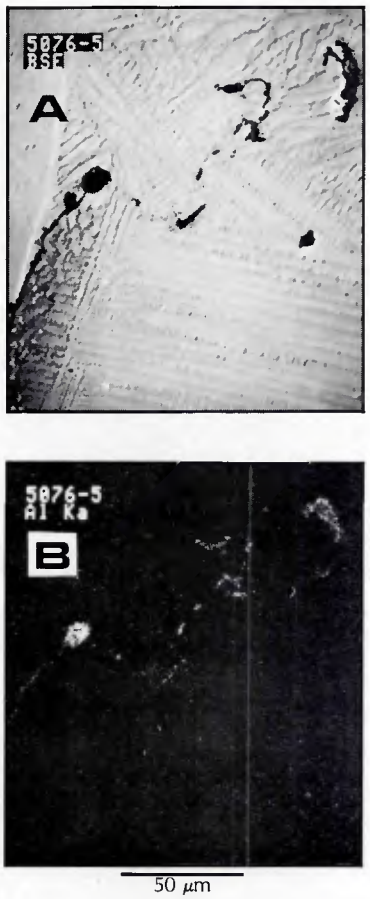

Fig. 6 — A — Scanning electron photomicrograph of a typical oxide tail (weld cross-section) showing the combined morphologies: crack-like stringers and spherical porosity (500X). B — Energy dispersive x-ray dot map for aluminum showing a heavy concentration with direct correlation to the discontinuity geometry (500X)

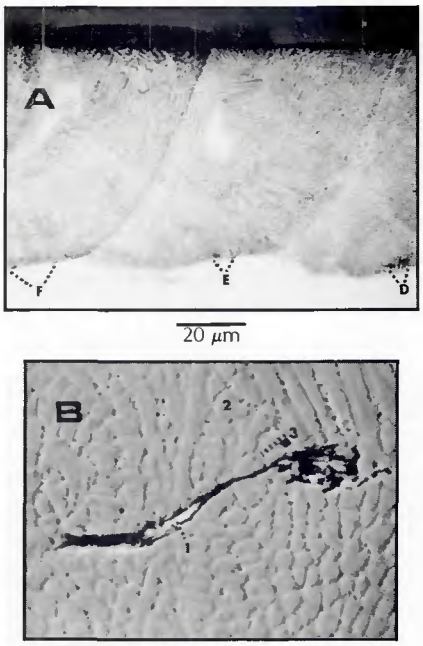

Fig. 7 — A — Longitudinal photomicrograph of a representative weld section showing the morphology of the oxide tail discontinuities located at positions D, E and F (25X). B — Scanning electron photomicrograph of the discontinuity at position F, above, showing the locations subjected to electron microprobe analysis

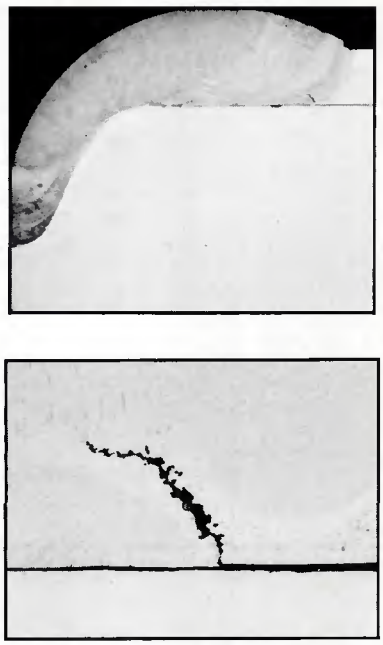

Fig. 8 — Photomicrographs of a representative weld cross-section showing the liquation zone cracking initiating at the cladding inner wall in the weld underbead region. Top — 25X; Bottom — 250X.

regions for subsequent destructive analysis.

Figure 9 shows the metallographic planes used to evaluate and analyze the cracking, and also a typical crack exposed by this procedure. Notice that the crack shown appears to extend into the weld fusion zone. However, close examination reveals that the liquation zone swirls up into the apparent fusion zone along an uneven melt boundary produced by the pulsed GTA welding technique. Also shown is a section of liquation zone porosity (lower right corner — Fig. 9B).

Figure 10 shows a typical crack, which apparently extends from a cored structure within the liquation zone. Analysis by EM performed in the regions marked indicated that Nb, Mo and Si were enriched in the cored phase (Position 8 — Fig. 10B), as compared to the primary dendrite (Position 10 — Fig. 10B). Analysis by SEM-EDS revealed very similar results, with the primary segregant being Nb, as shown in Fig. 11.

Liquation-zone porosity (Fig. 9) was very closely linked to the liquation-zone crack discontinuities. Figure 12 shows a representative region of the porosity discontinuity and a definite indication that this discontinuity was directly associated with the dissociation of base metal precipitates. Analysis by EM of the regions indicated within Fig. 12B revealed that the compositions of Areas 5 and 7 were nearly identical, and enriched with Nb, Mo and Si, as compared to the composition at the spot indicated as Position 6. This compositional difference is similar to that reported for the liquation-zone cracking and was a consistent result revealed by the many such discontinuities analyzed during this investigation.

Discussion

The preceding data indicate that the oxide tails were formed by the rejection of slag from the molten weld metal. Review of the weld metal composition (Table 2) reveals that a significant aluminum loss occurred during welding. Figure 13 shows a typical slag residue which randomly formed on the top surface of these welds. The SEM wavelength dispersive spectroscopy (WDS) of these small slag residues revealed high concentrations of Al, Ti and Ca — Fig. 13. Similarities in slag composition and that of the oxide tails, along with Al losses in the weld composition, lend credence to the postulate that the oxide tails are promoted by Al slag rejection to the free surfaces of the molten weld metal (*i.e.*, lap interface and top surface). This postulate is also cited in the literature (Ref. 4) and is assumed to result from: excessive joint clearances, inadequate inert gas shielding, or poor preweld cleaning.

Figure 14 is a schematic drawing of an end fitting used to examine the aforementioned joint clearance contribution. If the oxide tails were formed by a slag rejection phenomenon, then pre-placed joint clearances should increase their frequency and severity. This is, in fact, what occurred. When the joint clearance between the end fitting and the cladding was 0.13 mm (0.005 in.) or greater, the occurrence of oxide tails was significantly increased.

Another important procedural concern is the preweld cleaning procedure. A vigorous chemical etch (HNO_3-HF acids) that produced a bright metallic finish was found to reduce the occurrence of oxide tails. Kiser (Ref. 5) has supplied the authors with several examples of similar discontinuities and indicated that preweld cleaning to remove surface oxides, along with limited post-cleaning storage time to prevent room temperature oxidation, are effective methods for the prevention of oxide tail formation.

In this application, the combination of an interference fit between the cladding and the end fitting and very aggressive cleaning procedures was effective in reducing (not eliminating) the occurrence of oxide tails. An additional precaution would have been to add an inert gas

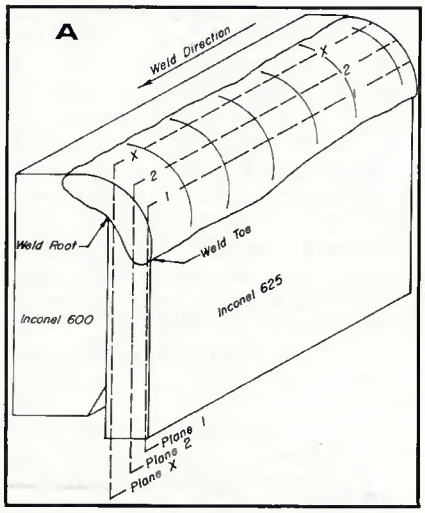

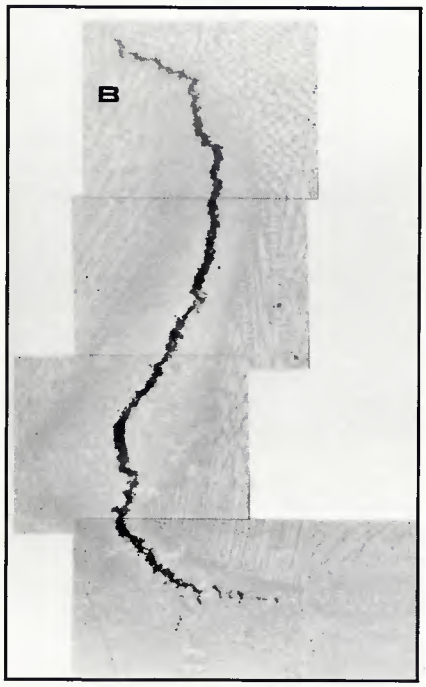

Fig. 9 — A — Schematic of the metallographic sections used to evaluate the cracking by longitudinal sectioning. B — Composite photomicrograph showing typical liquation zone crack and shrinkage porosity (arrow) discontinuities. Notice that the crack appears to extend into the cellular dendritic weld microstructure, but is in fact only resident in the cored microstructure typical of the liquation zone (500X)

shield to the back side of the weld. This precaution was not possible in this instance, due to the presence of the nuclear fuel package, and was therefore not evaluated.

Liquation-zone defects (cracking and porosity) were shown to coincide with the segregation of Nb, Mo and Si and were directly linked to the dissociation of the base metal precipitates in the NO6625. Data were presented to show

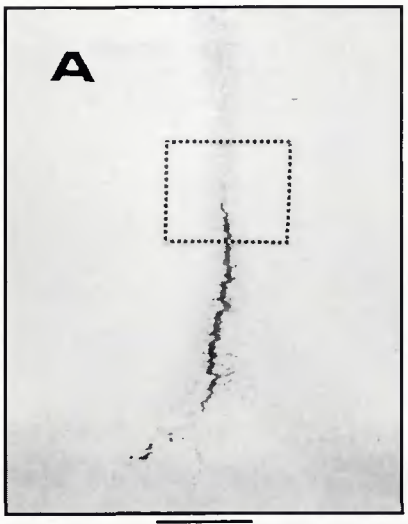

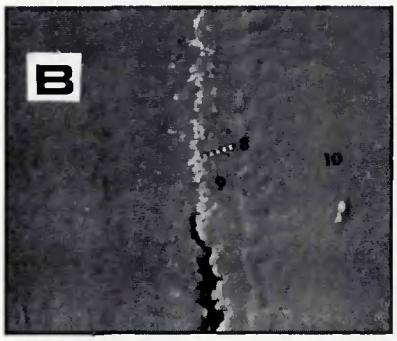

Fig. 10 — A — Scanning electron photomicrograph of a representative liquation-zone crack. B — Higher magnification scanning electron photomicrograph of the crack showing the crack tip, which appears to extend from a cored structure. Numbers identify locations used in the electron microprobe analysis

that the NO6625 alloy had a 40°C (72°F) gap between the nil-strength (1250°C/2282°F) and the solidus (1288°C/2350°F) temperatures. It was also shown that the solidus temperature of the NO6625 was below that of either the weld metal (1318°C/2404°F) or the NO6600 (1328°C/2422°F).

This data indicates that hot cracking has occurred and is supportive of the mechanisms proposed by previous investigators (Refs. 6–9). These theories rely upon two basic phenomena leading to cracking: (1) the formation of subsolidus liquid films, which wet the grain boundaries, and (2) the inability of these liquated grain boundaries to withstand the imposed strain from weld metal solidification.

Dissociation of the NO6625 precipitates to form a liquated region was demonstrated here and is proposed to be the cause of the subsolidus cracking. This hypothesis is supported by the Gleeble and DTA results, which show that the nil-strength temperature was below the solidus temperature for NO6625. Ow-

Fig. 11 — A — Scanning electron photomicrograph showing a representative liquation-zone crack. The light line running horizontally corresponds to the path followed by the energy dispersive spectroscopy trace. B — Energy dispersive analysis for niobium showing an increase in concentration adjacent to the crack edges

czarski and Duvall (Refs. 8, 9) reported similar results for nickel-based alloys, including metallographic evidence of carbide decomposition leading to liquation-zone defects.

Enrichments of Nb, Ti and Mo have been reported by several investigators to cause liquation-zone cracking (Refs. 8–12), supporting the negative contribution of Nb segregation in NO6625. Presumably, the Nb enrichment is promoted by a mechanism termed constitutional liquation (Ref. 7), which hypothesizes the development of liquid grain boundary films through a non-equilibrium redistribution of solute. A suggested catalyzing effect of silicon on carbide decomposition has been reported (Ref. 13), and is supported by the analytical data presented here. Therefore, it appears that expla-

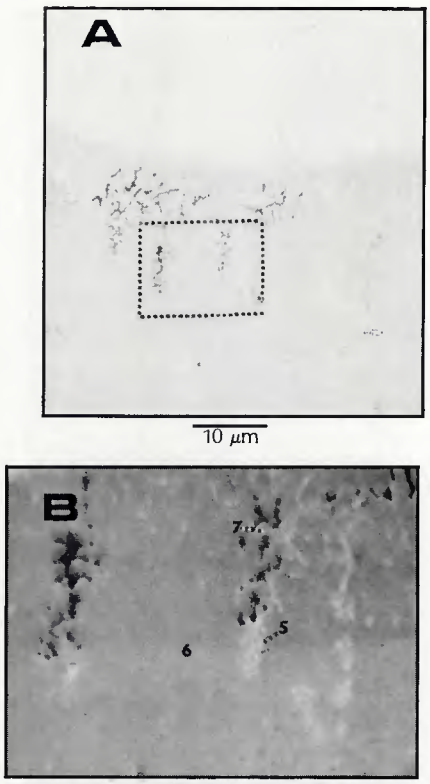

Fig. 12—A—Optical photomicrograph of a representative cross-section of the liquation zone shrinkage porosity discontinuity. Note the apparent dissociation of NO6625 precipitates leading directly into the liquation zone and the defect (100X). B—Scanning electron photomicrograph of the discontinuity shown above with numbered locations relating to the positions where electron microprobe analysis was performed

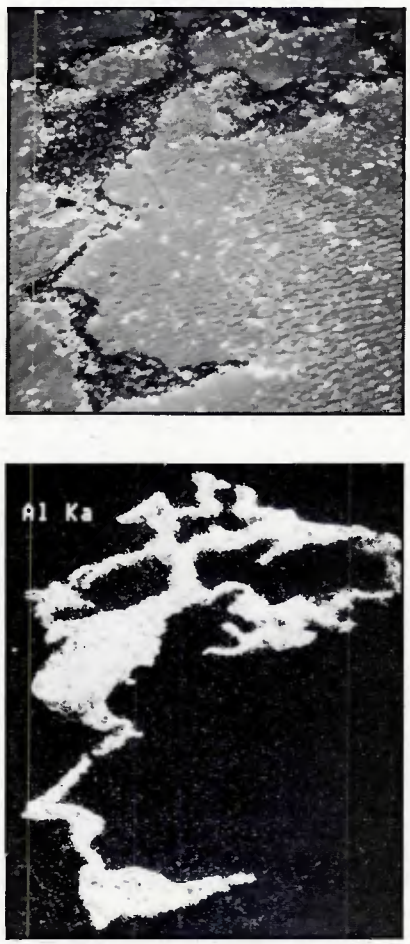

Fig. 13—Scanning electron photomicrograph of a typical slag that formed on the surface of the end fitting-to-cladding welds. The wavelength dispersive spectrum for aluminum is included to indicate that these slags were principally composed of aluminum compounds (300X)

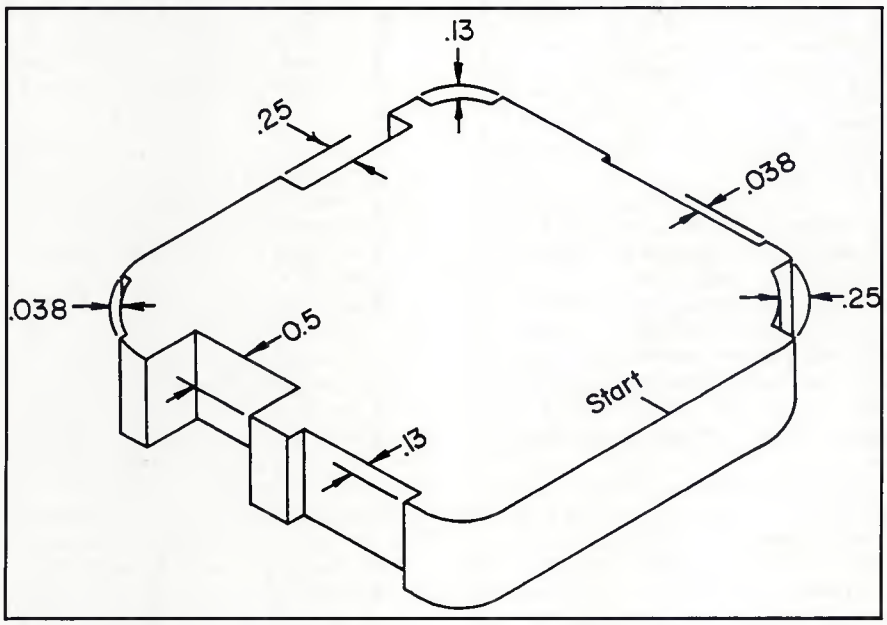

Fig. 14—Schematic of the end fitting used to evaluate the contribution of joint clearances to the formation of oxide tails

nation for the cracking observed during this study is consistent with the mechanisms reported for similar alloys.

However, the apparent similarities between cracking and porosity have not been previously reported. It is suggested that the two discontinuities are promoted by an identical set of compositional effects, but develop the different defect morphologies due to a difference in the imposed strain. This point is only postulated, since actual measurements of strain distribution were not attempted.

Procedural measures suggested to alleviate the tendency for liquation-zone discontinuities are:

1. Close control on the base metal composition (Refs. 1, 12).
2. Avoid large recrystallized grain sizes (ASTM 5 or greater) (Refs. 12, 14, 15).
3. Use low average heat input welding (Refs. 8, 14, 15).
4. Repair weld the affected area (Ref. 1).

Unfortunately, suggested recourses numbered 1 and 2 were not possible in this program. The starting materials were purchased in sufficient quantities to produce all requested hardware and could not be replaced within programmatic economic and schedule restraints. Also, the claddings were fabricated by another facility contracted by Argonne National Laboratory, and alterations to the thermomechanical processing history were not within the control of the welding organization. It should be noted that the material characterization indicated that the NO6625 did not have an excessively large grain size, and therefore, it is assumed that the prior thermomechanical processing history satisfactorily complied with the welding concerns.

Improvements to the welding procedure relating to low heat input processes were evaluated in a circuitous fashion. Figure 15 shows a representative weld used in the fabrication of the NO6625 cladding. This longitudinal weld was produced by conventional gas tungsten arc welding using standard welding fixtures. Notice that the transition between the fusion zone and base material does not exhibit extensive grain boundary liquation. Explanations for the difference in this weld and those demonstrating a susceptibility to liquation can be assumed to result from two procedural differences: (1) the longitudinal weld was performed with comparable average current values but at a speed six times faster than the end-fitting-to-cladding weld, and (2) the continuous current weld produces a more consistent steady-state temperature gradient. Obviously, the lower heat input produced by the welding procedure for the longitudinal weld helped to circumvent the tendency for liquation.

Fig. 15 — Top — Photomicrograph of the longitudinal gas tungsten arc weld used to fabricate the NO6625 cladding (10X). Bottom — Increased magnification view of the longitudinal weld showing the absence of liquation or precipitate dissociation adjacent to the fusion zone (250X)

However, the more subtle point of temperature gradient requires further explanation.

Review of Figure 3 shows the weld chill and clamp fixturing used for the end-fitting-to-cladding weld. Notice the gaps between the finger-like fixture segments. Each example of liquation-zone cracking or shrinkage porosity found in these evaluations occurred at the point where a gap existed in the chill fixture. Observation also revealed that each of these discontinuities was associated with an increase in the apparent fusion zone size, indicating an effective decrease in heat sink efficiency and a change in the local temperature gradient. Thus, the decrease in heat sink efficiency is assumed to be a contributor through an assumed increase in the temperature adjacent to the weld.

Apparently, the welding procedure used in this program produced a situation that was very close to a critical point where cracking occurred. Transition between good and bad welds was dependent upon a threshold in combined effects relating to the volume fraction of precipitate intercepted and the thermal cycle. Since the material composition variable was uncontrollable, the only resolution to this difficulty was to produce a more consistent thermal cycle. When all gaps in the chill fixturing were reduced from approximately 3 mm (0.12 in.) to a value less than 1 mm (0.04 in.), the propensity for cracking disappeared.

However, another contributor to the variable thermal cycle, pulsed current welding, was also assumed to be at least partially responsible for the production of these discontinuities. Liquation is promoted by the nonequilibrium redistribution of a solute due to rapid thermal cycles (Ref. 7). Pulsed current welding should accentuate this phenomenon, since the heat is applied in an incremental fashion, producing steep temperature gradients. Secondly, the transitions from melt to solidification, to remelt and resolidification, produced by GTAW-P tend to effectively increase the local strain imposed on the previous weld event. Review of the crack morphology (Figs. 6 and 9) reveals that the cracks appeared to extend into the fusion zone. In fact, this extension was related to the interface between the overlapping weld events, characteristic of pulsed current welding. Thus, the observations made here tend to indicate that GTAW-P increases the sensitivity to liquation-zone cracking. This observation is supported by similar observations reported previously (Ref. 16).

Finally, attempts to repair these defective welds by manual GTA welding were completely unsuccessful. This is converse to assumed beneficial effects of filler metal. Utilization of filler metal (Inconel 82) to produce a more compliant and perhaps lower solidus temperature weld metal produced a pronounced increase in cracking susceptibility. Results published by Yeniscavich (Ref. 15) indicate that multipass welds on NO6600 using Inconel 82 filler metal were susceptible to cracking in the reheated passes, and as such, are very consistent with what was experienced during this work.

Conclusions

1. Oxide tail discontinuities in NO6625 to NO6600 pulsed GTA welds resulted from the rejection of aluminum slag from the molten weld metal.

2. The occurrence of oxide tails can be reduced by the utilization of interference fits for lap joints and aggressive chemical cleaning.

3. Liquation-zone cracking and shrinkage porosity were found to result from the decomposition of carbides (primarily niobium carbides), resulting in an enrichment of niobium in the cored-liquation-zone structure.

4. The nil-strength temperature of NO6625 is 1250°C (2282°F), which is approximately 40°C (72°F) below the solidus temperature (1288°C/2350°F), supporting the hypothesis of a hot cracking mechanism.

5. Low heat input welding and uniform heat sinking reduce the tendency for liquation-zone discontinuities.

6. Repair welding is not recommended as a solution when liquation-zone discontinuities are prevalent.

Acknowledgments

The authors acknowledge the valuable assistance of the following people: Dr. K. W. Mahin of the Lawrence Livermore National Laboratory for performing the hot strength testing, and Gloria A. Romero for typing the manuscript. Work was performed under the United States Department of Energy contract W7405-Eng36.

References

1. Prager, M., and Shira, C. S. February 1968. Welding of precipitation-hardening nickel base alloys. WRC Bulletin 128.

2. Standard methods for determining average grain size. 1983. *Annual Book of ASTM Standards*. ASTM, Vol. 03.03, pp. 121–155.

3. *Huntington Alloys Handbook*. 1970. Huntington Alloys, Inc., Huntington, West Virginia, 5th edition.

4. *Metals Handbook*. 1971. ASM, Metals Park, Ohio, 8th edition, Vol. 6, p. 289.

5. Personal communication. Kiser, S., Huntington Alloys, Inc.

6. Borland, J. C., and Younger, R. N. 1960. Some aspects of cracking in welded Cr-Ni austenitic steels. *British Welding Journal* 7(1):22–59.

7. Pepe, J. J., and Savage, W. F. Effects of constitutional liquation in 18 Ni maraging steel weldments. *Welding Journal* 46(9):411-s to 422-s.

8. Owczarski, W. A., Duvall, D. S., and Sullivan, C. P. 1966. A model for heat-affected zone cracking in nickel-base superalloys. *Welding Journal* 45(4):145-s to 155-s.

9. Duvall, D. S., and Owczarski, W. A. 1967. Further heat-affected zone studies in heat resistant nickel alloys. *Welding Journal* 46(9):423-s to 432-s.

10. Robinson, J. L., and Scott, W. H. 1980. Liquation zone cracking during the welding of austenitic stainless steel and nickel alloys. *Phil. Trans. R. Soc. Lond.* A295, pp. 105–107.

11. Thompson, E. G. 1969. Hot cracking studies of Alloy 718 weld heat-affected zones. *Welding Journal* 48(2):70-s to 79-s.

12. Thompson, R. G., Cassimus, J. J., Mayo, D. E., and Dobbs, J. R. 1985. The relationship between grain size and microfissuring in Alloy 718. *Welding Journal* 64(4):91-s to 96-s.

13. Cieslak, M. J., and Savage, W. F. April 1984. Hot cracking investigation of Alloy CN-7M. Presented at the 65th Annual AWS Convention, Dallas, Tex.

14. Lingenfelter, A. C., and Shoemaker, L. E. June 1984. Weld induced base metal microfissuring in high temperature alloys. Lawrence Livermore National Laboratory Report UCRL 91062.

15. Yeniscavich, W. 1966. A correlation of Ni-Cr-Fe alloy weld metal fissuring with hot ductility behavior. *Welding Journal* 45(8):344-s to 356-s.

16. Patterson, R. A., and Milewski, J. O. 1985. GTA weld cracking — Alloy 625 to 304L. *Welding Journal* 64(8):227-s to 231-s.